The Journal of CPRI,
Vol. 10, No. 1, March 2014 pp. 107-118

High Efficient Soft Switching Cuk Converter with Ripple Correlation Control MPPT for PV Applications

Mutta Krishna Murthy*, Sandeep N** and Kulkarni P S***

This paper presents the application of "ripple correlation control (RCC)" maximum power point tracking (MPPT) algorithm for photovoltaic (PV) system employing dc-dc Cuk converter to maximize the output power of PV module. Soft switching commutation of the main and auxiliary switches at zero-voltage using active clamp technique allows the operation of the Cuk converter at very high switching frequencies with reduced size of reactive elements and electromagnetic interference. The combination of auxiliary switch, clamp capacitor and resonant inductor is used to exploit the advantage of high efficiency with zero switching losses. RCC technique uses the high frequency signal ripple, which makes it to converge asymptotically to the maximum power point independent of module configuration and parameters. The operating modes of converter for different switching time intervals are analyzed and design considerations are presented. The simulated performance of the converter with RCC MPPT over conventional MPPT algorithms is presented. The MPPT methods are compared on the basis of the time taken to track the maximum power point (MPP), steady state oscillations about MPP and dependence on array parameters. To evaluate the viability of ZVS Cuk converter with RCC MPPT, the entire system is simulated using MATLAB/SIMULINK platform for an 87 Wp solar PV system.

Keywords: *Active clamping, DC-DC Cuk converter, Photovoltaic system, Ripple correlation control (RCC), Zero voltage switching (ZVS).*

NOMENCLATURE

V_s	:	Converter input voltage (V)
V_o	:	Converter output voltage (V)
L_1	:	Input inductor (H)
L_2	:	Output inductor (H)
C_a	:	DC capacitor (F)
C_o	:	Output capacitor (F)
L_r	:	Resonant inductor (H)
I_o	:	Output current (A)
f_s	:	Switching Frequency (Hz)
L_n	:	Normalized load current
β	:	Normalized clamping voltage
C_r	:	Resonant capacitor (F)
w_o	:	Resonant frequency (rad/sec)
V_{oc}	:	Open circuit voltage (V)
C_c	:	Clamp capacitor (F)
V_{s1}	:	Voltage across main switch (V)
I_{s1}	:	Current through main switch (A)
V_{s2}	:	Voltage across auxilary switch (V)
I_{s2}	:	Current through auxilary switch (A)
V_c	:	Voltage across clamp capacitor (V)
I_{Lr}	:	Resonant inductor Current (A)

*PG Student, Department of Electrical Engineering, VNIT, Nagpur, India. E-mail: kittu237@gmail.com
**PG Student, Department of Electrical Engineering, VNIT, Nagpur, India. E-mail: sandeepbabu28@gmail.com
***Associate Professor, Department of Electrical Engineering, VNIT, Nagpur, India. E-mail: pskulkarni@eee.vnit.ac.in

I_{Dfw} : Current through Diode D_{fw} (A)

V_{Dfw} : Voltage across Diode D_{fw} (V)

I_s : Source current (A)

V_{MPP} : Maximum power point voltage (V)

I_{MPP} : Maximum power point current (A)

P_M : Peak power of panel (W)

I_{sc} : Short circuit current (A)

K_V : Temperature coefficient of V_{oc} (V/°C)

K_I : Temperature coefficient of I_{sc} (A/°C)

R_s : Parasitic series resistance (Ω)

R_p : Parasitic parallel resistance (Ω)

G_n : Nominal insolation (= 1000 W/m^2)

T_n : Nominal cell temperature (= 25°C)

a : Diode ideality factor (= 1.2-2)

1.0 INTRODUCTION

Now a days the unavailability of conventional energy sources like petroleum, energy crisis due to the growing demand and increasing concerns about the environmental conservation has led to the use of alternate energy sources in power generation that are cleaner and renewable [1]. Photovoltaic (PV) energy is presently considered to be one of the most useful natural energy sources since it is free, abundant, pollution-free and distributed throughout the earth. Despite all the above mentioned advantages of generating energy using solar PV system, the efficiency of energy conversion is low, since it is affected by so many factors such as insolation, temperature, dirt, shadow and so on.

The PV panel exhibits non-linear power-voltage characteristics as shown in Figure 1. Thus, in order to achieve maximum efficiency it becomes necessary to extract the maximum power from these panels using suitable power conditioning system (PCS). The PCS must keep the power extracted from the PV panel close to the MPP. Several solutions for a PCS with MPPT capability have been proposed from time to time [2]. Some of the popular techniques are the hill climbing method, incremental conductance method, constant voltage method, β method and the RCC method. PCS consists of a dc-dc converter whose duty cycle is varied in accordance with the changes in environmental conditions to keep the system operating point near MPP. Among all the dc-dc converters the Cuk converter [3] is considered to be best suited whose operating region is as shown in Figure 2.

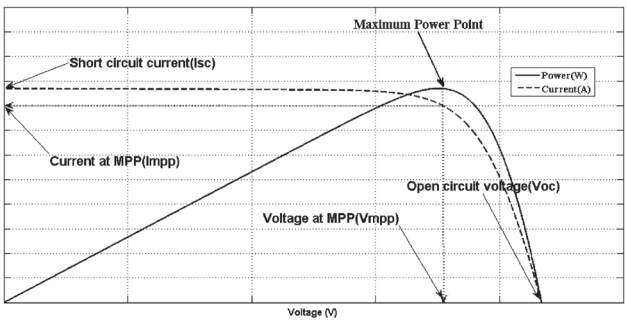

FIG. 1 CHARACTERISTIC CURVES OF PV MODULE

Change in the duty cycle enables it to operate through I_{sc} to V_{oc} with zero non-operating zone [4]. The operation of Cuk converter at high frequency reduces the size of reactive components and cost. However this results in the reduced efficiency of the converter due to increased switching losses, which can be reduced substantially by use of soft commutation techniques like ZVS and zero current switching.

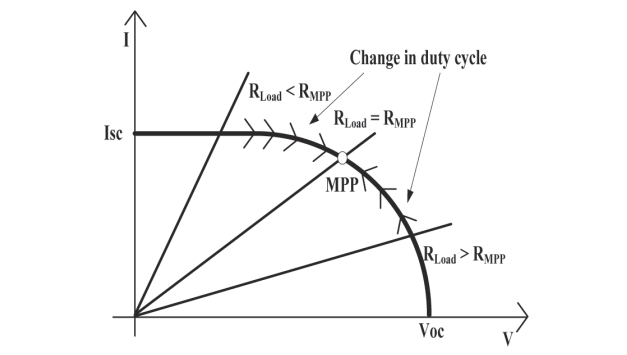

FIG. 2 OPEARTIONAL REGIONS OF THE I-V CURVE FOR CUK CONVERTER

In this paper a high efficient PCS based on active clamping dc-to-dc Cuk converter for tracking MPP of PV module is proposed. The major parasitic reactances like transistor output capacitance, track inductance are absorbed in this converter. The performance of converter with

RCC MPPT is compared with perturb and observe (P&O), incremental conductance MPPT methods based on the parameters like transient tracking time, speed and power ripple near MPP. Results demonstrating the comparative performance are presented. A table that summarizes the major characteristics of the MPPT methods as applied to ZVS Cuk converter is also provided. Validation of the performance comparison is done based on the simulation of MPPT methods with the proposed system in MATLAB/SIMULINK environment.

2.0 SYSTEM MODELING

Figure 3 shows the 87 W_p solar PV panel with ZVS Cuk converter based PCS with RCC MPPT algorithm. The proposed system has been modelled as under.

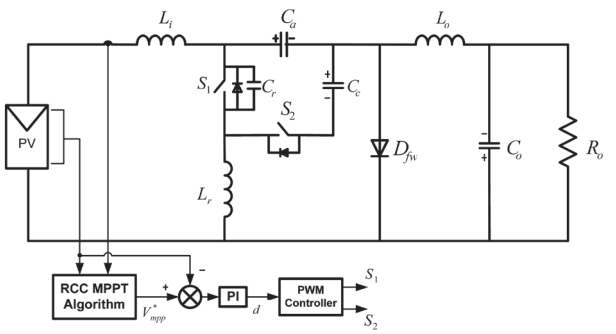

FIG. 3 ZVS CUK CONVERTER BASED PV SYSTEM

2.1 PV Panel Modeling

The simplified electrical model of PV module is current source in parallel with a diode. Series (Rs), Parallel (Rp) resistances are included to obtain a practical PV model for simulation studies [5] as shown in Figure 4.

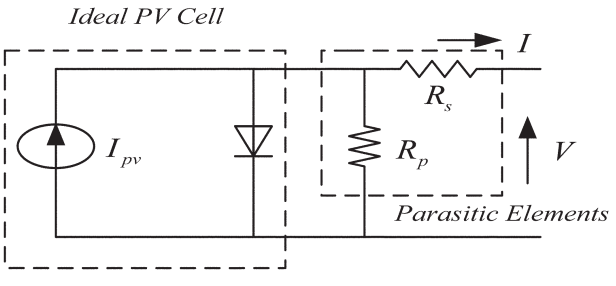

FIG. 4 EQUIVALENT CIRCUIT OF PV MODULE

The main equation for the output current of PV module is

$$I = I_{PV} - I_0\left[\exp\left(\frac{V+R_sI}{V_t a}\right)-1\right]-\frac{V+R_sI}{R_p} \quad ....(1)$$

Where I_{PV} and I_0 are cell photovoltaic and diode leakage currents respectively, V is the output voltage across module, Vt = NskT/q is the thermal voltage of the module with Ns cells connected in series, k is Boltzmann constant (1.38×10-23 J/K), q is charge of electron (1.6×10-19 C) and T (in Kelvin) is the temperature of the module.

The cell photovoltaic current is caluculated from

$$I_{PV} = \left(I_{PV,n} + K_I\Delta T\right)\frac{G}{G_n} \quad ....(2)$$

and diode leakage current is computed from

$$I_0 = \frac{I_{SC,n} + K_I\Delta T}{\exp\left(\left(V_{oc,n} + K_V\Delta T\right)\Big/ aV_t\right)-1} \quad ....(3)$$

The key electrical specifications of chosen PV module are tabulated in Table 1.

TABLE 1

KC85T PV MODULE ELECTRICAL SPECIFICATIONS

Parameter	Symbol	Values
Maximum power	P_M	87 W
Peak power voltage	V_{MPP}	17.4 V
Peak power current	I_{MPP}	5.02 A
Open circuit voltage	V_{OC}	21.7 V
Short circuit current	I_{SC}	5.34 A
Temperature coefficient of V_{oc}	K_V	-8.21×10^{-2} V/° C
Temparature coefficient of I_{sc}	K_I	2.12×10^{-3} A/° C

2.2 Circuit Description

The circuit diagram of the ZVS Cuk converter with RCC MPPT is as shown in Figure 3. Unlike the conventional Cuk converter an auxilary switch in series with clamp capacitor, a resonant

inductor L_r and resonant capacitor C_r are included to achieve soft commutation of the semiconductor switches [6]. To simplify the analysis the following assumptions are made

- All the semiconductor devices and reactive elements are ideal.
- The clamp capacitor C_c is selected to have large capacitance, which makes the voltage across it to be a constant value.
- The input and output filter inductances are assumed to be large enough to consider them as a current source I_s and I_o respectively.
- Sufficient energy is stored in resonant inductor L_r to discharge C_r completely for the soft commutation of switch S_1.

The circuit behavior with the help of six topological stages of operating modes and the key waveforms during one switching cycle is shown in Figure 5 and Figure 6 respectively.

Mode 1: (t_o - t_1) -: Figure 5(a) shows the operating state of the converter during this interval. Prior to t_o, the main switch S_1 is on, auxiliary switch and diode D_{fw} are off. At $t=t_o$ the switch S_1 is turned off with zero switching loss, and the capacitor C_r starts charging linearly and it reaches to $V_{ca}=V_o$(output voltage) + V_s(voltage across PV module) at the end of this mode. The equations that describe this state are:

$$I_{Lr}(t) = I_o + I_s \quad ....(4)$$

$$V_{Cr}(t) = \frac{(I_s + I_o)*(t_1 - t_0)}{C_r} \quad ....(5)$$

$$\Delta t_1 = \frac{V_{Ca} * C_r}{(I_s + I_o)} \quad ....(6)$$

Mode 2: (t_1 – t_2) -: Figure 5(b) shows the operating state of the converter during this interval. When V_{cr} reaches V_{ca}, the free-wheeling diode D_{fw} becomes biased and starts conducting. The current through L_r and voltage V_{cr} involve in a resonant way and V_{cr} rises from V_{ca} to (V_{ca}+V_c). The voltage across C_r is clamped to (V_{ca}+V_c) and the equations describing this state are:

$$I_{Lr}(t) = (I_s + I_o)\cos w_o(t - t_1) \quad ....(7)$$

$$V_{Cr}(t) = V_{Ca} + (I_s + I_o) z_o \sin w_o(t - t_1) \quad ....(8)$$

$$z_o = \sqrt{\frac{L_r}{C_r}} \quad ....(9)$$

$$w_o = \frac{1}{\sqrt{L_r C_r}} \quad ....(10)$$

$$\Delta t_2 = t_2 - t_1 = \frac{1}{w_o} \sin^{-1}\left(\frac{V_C}{(I_S + I_O) z_o}\right) \quad ....(11)$$

Mode 3: (t_2– t_3) -: Figure 5(c) shows the operating state of the converter during this interval. As Vcr=(V_{ca}+V_c) the antiparallel diode of S_2 starts conducting. The current through L_r ramps down as C_c is considered as a constant voltage source, until it reaches zero and rises again when it changes its direction. At the end of this stage the current through the inductor is equal to -(I_s+I_o) and switch S_2 is turned off. The equations that describe this state are:

$$I_{Lr}(t) = \frac{-V_C}{L_r}(t - t_2) + (I_s + I_o)\sqrt{1 - \left(\frac{V_C}{(I_s + I_o) z_o}\right)^2} \quad ....(12)$$

$$V_{Cr}(t) = V_{Ca} + V_C \quad ....(13)$$

$$\Delta t_3 = t_3 - t_2 = \frac{-(I_s + I_o) L_r}{V_C}\left(1 + \sqrt{1 - \left(\frac{V_C}{(I_s + I_o) z_o}\right)^2}\right) \quad ....(14)$$

Mode 4: (t_3– t_4) -: Figure 5(d) shows the operating state of the converter during this interval. The voltage across C_r falls due to the resonance between L_r and C_r. At the end of this stage the voltage across the capacitor C_r becomes zero and the antiparallel diode of S_1 starts conducting. The equations that describe this state are:

$$I_{Lr}(t) = \frac{V_c}{z_o}\sin w_r(t - t_3) - (I_s + I_o)\cos w_r(t - t_3) \quad ....(15)$$

$$V_{Cr}(t) = V_{Ca} + (I_s + I_o) z_o \sin w_r(t - t_3) + V_c \cos w_r(t - t_3) \quad ....(16)$$

$$\Delta t_4 = t_4 - t_3 = \frac{1}{w_r}\left(\cos^{-1}\left(\frac{-V_{Ca}}{\sqrt{(I_3 z_o)^2 + (V_c)^2}}\right) + \tan^{-1}\left(\frac{-(I_s + I_o) z_o}{V_c}\right)\right)$$

....(17)

Mode 5: ($t_5 - t_6$) -: Figure 5(e) shows the operating state of the converter during this interval. At this stage S_1 turns on with zero losses (ZVS), since V_{cr} is equal to zero. The current through L_r changes its polarity and ramps up to reach I_s at the end of this stage. The equations describing this state are given as follows:

$$I_{Lr}(t) = \frac{V_s}{L_r}(t - t_4) + I_{Lr}(t_4) \quad ....(18)$$

$$V_{Cr}(t) = 0 \quad ....(19)$$

$$\Delta t_5 = t_5 - t_4 = \frac{\left(I_s - I_{Lr}(t_4)\right)L_r}{V_s} \quad ....(20)$$

Mode 6: ($t_6 - t_7$) -: Figure 5(f) shows the operating state of the converter during this interval. The free-wheeling diode D_{fw} becomes reverse biased and turns off with zero switching loss. Power is transferred to the load through S_1 carrying a current equal to I_s+I_o. The auxiliary switch is off and the stage ends when S_1 is turned off with ZVS at the end of switching cycle and the circuit goes to operating mode-1. In this operating mode the key voltages and currents of the circuit are expressed as follows:

$$I_{Lr}(t) = (I_s + I_o) \quad ....(21)$$

$$V_{Cr}(t) = 0 \quad ....(22)$$

$$\Delta t_6 = t_6 - t_5 = DT_s \quad ....(23)$$

3.3 General Design Considerations

As shown in Figure 6 the resonant time intervals are of short duration as compared to the time intervals of switching states 3, 5 and 6. The gain (q) of the converter is derived by averaging and equating the voltage across L_r to zero [7].

$$q = \frac{V_o}{V_s} = \frac{D - 2.L_n}{1 - D + 2.L_n} \quad ....(24)$$

$$L_n = \frac{L_r.I_o}{V_s.T_s} \quad ....(25)$$

The gain of the converter is a function of duty ratio (D) and L_n, T_s is the switching time interval. The current that flows in the clamping capacitor must be zero over a switching cycle to have the steady state operation of the converter. Thus

$$I_c = \frac{1}{T_s}\int_0^{(1-D)T_s}\left[\frac{-V_c}{L_r}t + I_s + I_o\right]dt = 0 \quad ....(26)$$

$$\beta = \frac{V_c}{V_s} = \frac{2L_n}{(1-D)}.\frac{1}{(1-D+2.L_n)} \quad ....(27)$$

The energy stored in the resonant inductor must be greater than the stored energy of the resonant capacitor during mode 3 to have a proper soft commutation of S_1 and S_2. We have

$$L_n \geq \left[\frac{(1-D)}{(1-D)T_s.w_o - 2}\right] \quad ....(28)$$

Where w_o is the resonant frequency, which is considered to be multiple of switching frequency. However in the practical realization of the converter, the maximum current of the input inductor is greater than the average current. Thus there is more energy stored to commutation. Thus (28) must have a correction factor.

$$L_{n_{\min}} \geq \left[\frac{2L_n}{1-D} + 1\right].\left[\frac{\eta}{(D - 2.L_n).\frac{r}{2} + 1}\right].\frac{1}{T_s.w_o} \quad ....(29)$$

Where η is the efficiency of the converter and r is the ripple current through the input inductor. For the soft commutation of switches, there should be time delay between the gating pulses of S_1 and S_2. Then

$$t_d \geq \frac{(V_c + V_o).C_r}{I_s} \quad ....(30)$$

$$t_d \leq \frac{(V_c + V_o).C_r}{I_s} + \frac{I_s.L_r}{(V_o + V_s)} \quad ....(31)$$

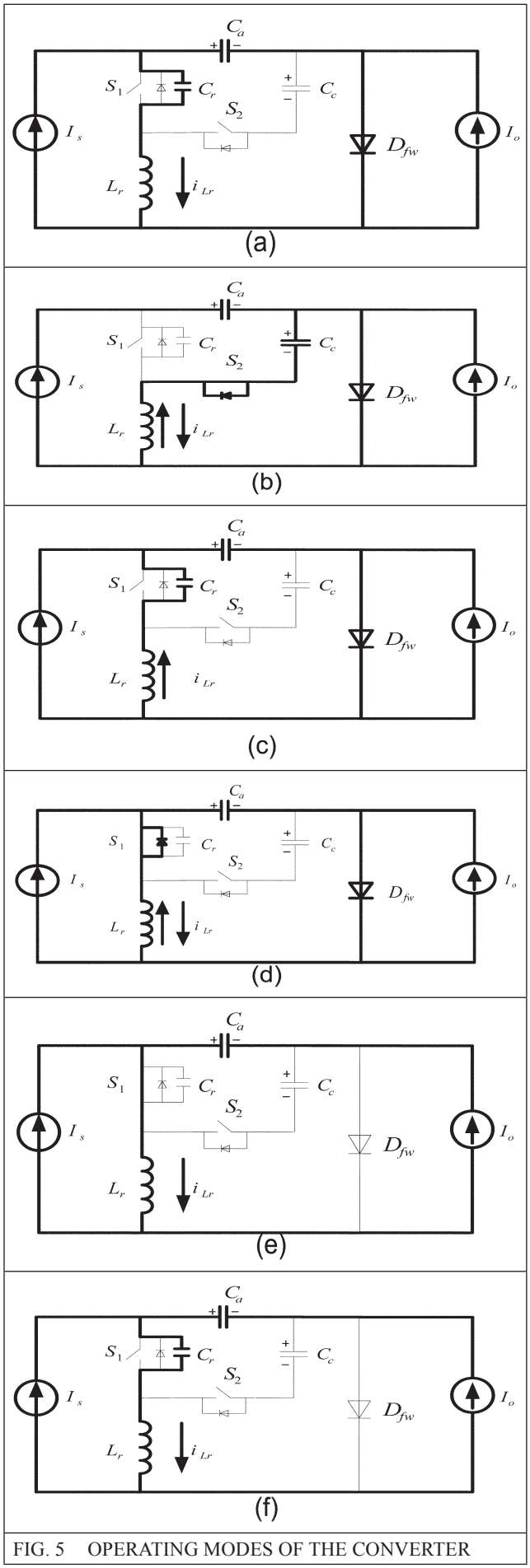

FIG. 5 OPERATING MODES OF THE CONVERTER

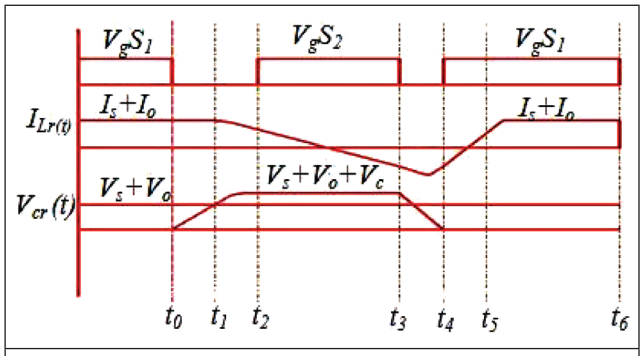

FIG. 6 KEY WAVEDORMS OF THE IDEAL CONVERTER

3.0 MPPT TECHNIQUES

The popular MPPT techniques like P&O, incremental conductance and RCC are discussed in foregoing sections [8]

3.1 Perturb and Observe (P&O)

This method involves a perturbation in the operating voltage of the PV panel by perturbing in the duty ratio of the PCS. The P & O method shown in Figure 7 operates by periodically incrementing or decrementing the output voltage of the PV panel and comparing the power obtained in the current cycle with the power of the previous one. From Figure 1 it can be seen that decrementing (incrementing) the voltage decreases (increases) the power when operating on the left of the MPP and increases (decreases) the power when on the right of the MPP. Subsequent perturbation should be kept the same if there is a increase in power and should be decreased if there is a decrease in power.

The process is repeated periodically untill the MPP is tracked and the system then oscillates about the MPP. Perturbation step size decides the range of oscillations about MPP. However a smaller perturbation size slows down the MPPT. P&O method can fail under rapidly chnaging atmospheric conditions.

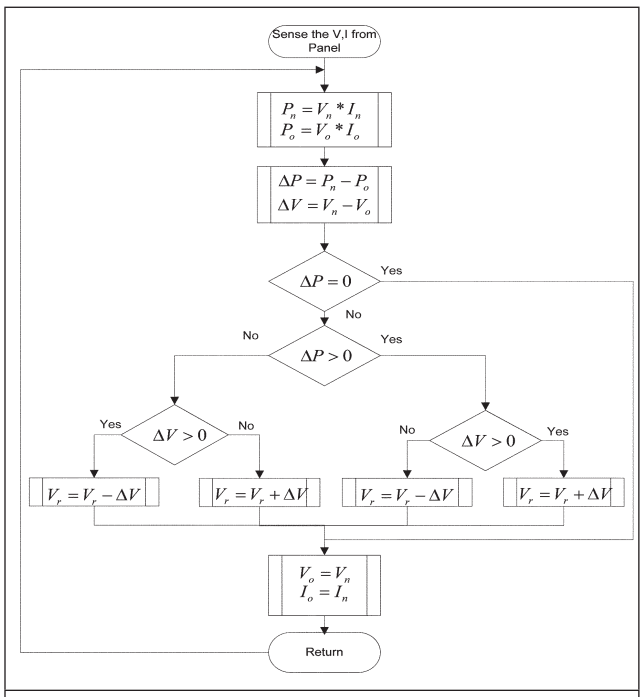

FIG. 7 FLOW CHART FOR P&O MPPT ALGORITHM

3.2 Incremental Conductance

The incremental conductance (IncCond) method is based on the fact that the slope of the PV panel Power-voltage curve (Figure 1) is zero at MPP, positive on the left of MPP and negative on the right given as

$$\begin{aligned} dP/dV &= 0 \quad \text{at MPP} \\ dP/dV &> 0 \quad \text{left of MPP} \\ dP/dV &< 0 \quad \text{right of MPP.} \end{aligned} \qquad \text{....(32)}$$

Since

$$\frac{dP}{dV} = I + V\frac{\Delta I}{\Delta V} \qquad \text{....(33)}$$

The MPP is tracked by comparing the instantaneous conductance (I / V) to the incremental conductance (ΔI / ΔV) as shown in the flow chart in Figure 8. In theory the steady state oscillations are eliminated once the derivative of power with respect to voltage is zero at MPP. However a zero value of the slope hardly ever occurs due to digital implementation. Effective way of performing the IncCond is to use the instantaneous conductance and the incremental conductance to generate an error signal. A simple proportional integral (PI) control can then be used to drive this error to zero.

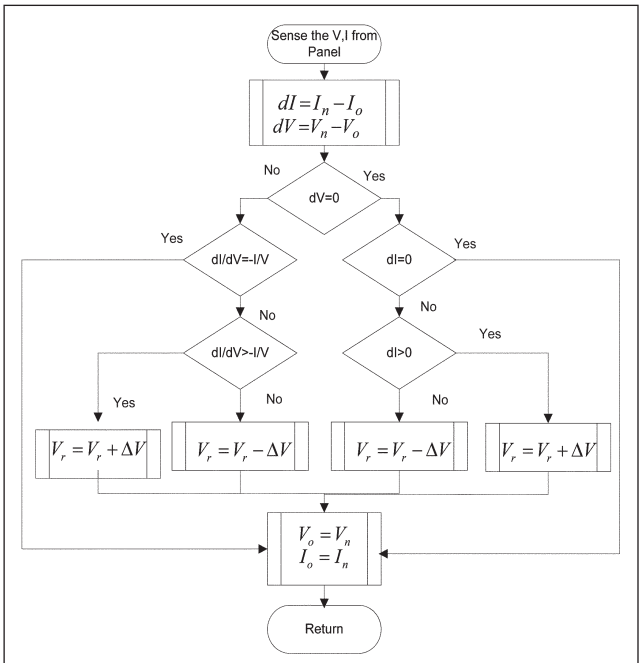

FIG. 8 FLOW CHART FOR INCCOND MPPT ALGORITHM

3.3 Ripple Correlation Control

When a PV panel is connected to a power electronic converter the switching action in the converter imposes current and voltage ripple on the PV panel. The RCC method is based on the principle of maximum power transfer, and it uses the oscillations to determine the MPP. RCC correlates the time derivative of the time-varying PV power with the time derivative of the time-varying PV voltage or current to drive the power derivative to zero, thus reaching the MPP.

$$\begin{aligned} \frac{dV}{dt}\frac{dP}{dt} > 0 &\Rightarrow V < V_{mpp} \\ \frac{dV}{dt}\frac{dP}{dt} < 0 &\Rightarrow V > V_{mpp} \end{aligned} \qquad \text{....(34)}$$

The derivatives in (34) are usally undesirable and hence these are approximated by high-pass filters with cutoff frequency higher than the ripple frequency. The sign of the time derivatives of power and voltage is computed and an integral controller is used to integrate the product which

determines the perturbation step size of the voltage reference. The gain K of the integral controller is tuned according to the requirement of speed and trajectory of convergence. The block diagram of RCC MPPT is as shown in Figure 9.

$$\Delta V_{dc} = k \int \frac{dp}{dt}\frac{dv}{dt}dt \quad \text{....(35)}$$

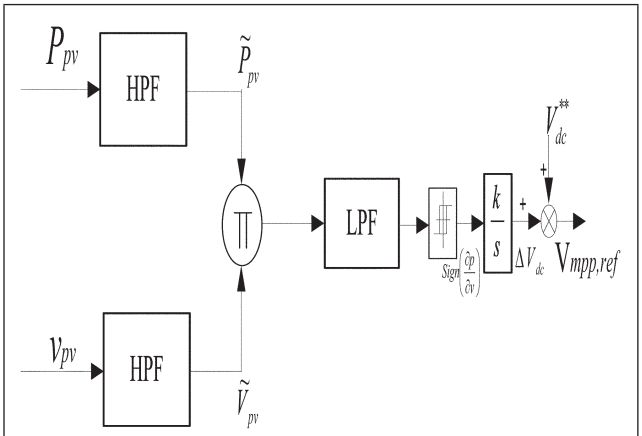

FIG. 9 BLOCK DIAGRAM OF RCC MPPT

4.0 PERFORMANCE RESULTS

In order to evaluate the performance of the ZVS-PWM converter with the selected MPPT techniques simulation is carried out using MATLAB/SIM–ULINK. The PV panel is modeled by using its electrical characteristics to provide the output voltage and current, which are fed to the converter and the controller simultaneously. The converter components are chosen according to the design considerations presented in section 3.0 and the values are tabulated in Table 2.

TABLE 2
PARAMETERS OF CUK CONVERTER

Parameter	Values
Output power (*P*)	87 W
Input voltage (V_S)	17.4 V
Output voltage (V_O)	52 V
Switching frequency (f_S)	50 kHz
Resonant frequency (f_r)	250 kHz
Input (L_i) and output (L_O) filter inductor	5.07 mH
Capacitor C_a (PV side)	1.81 µF
Capacitor C_o (output side)	0.5 µF
Resonant capacitor (C_r)	25.92 nF
Resonant inductor (L_r)	4 µH
Clamping capacitor (C_c)	5 µF
Duty ratio (*D*)	0.75
Gain (*q*)	2.98

To test the operation of the system, the condition of changing insolation is modeled. The level of insolation is varied between three levels. The first level is 1000 W/m^2; at t=0.02s, the level is suddenly changed to 600 W/m^2 at t=0.04s and then to 800 W/m^2 at t=0.06s. Output power of 87W, 51W and 69 W are the desired values of peak power at G= 1000 W/m^2, 600 W/m^2 and 800 W/m^2 respectively.

The main points that emerge out of the comparative application of the selected MPPT techniques are briefly discussed and summarized in Table 3 with respect to various performance parameters. The efficiency of converter for different loading is presented in Figure 17.

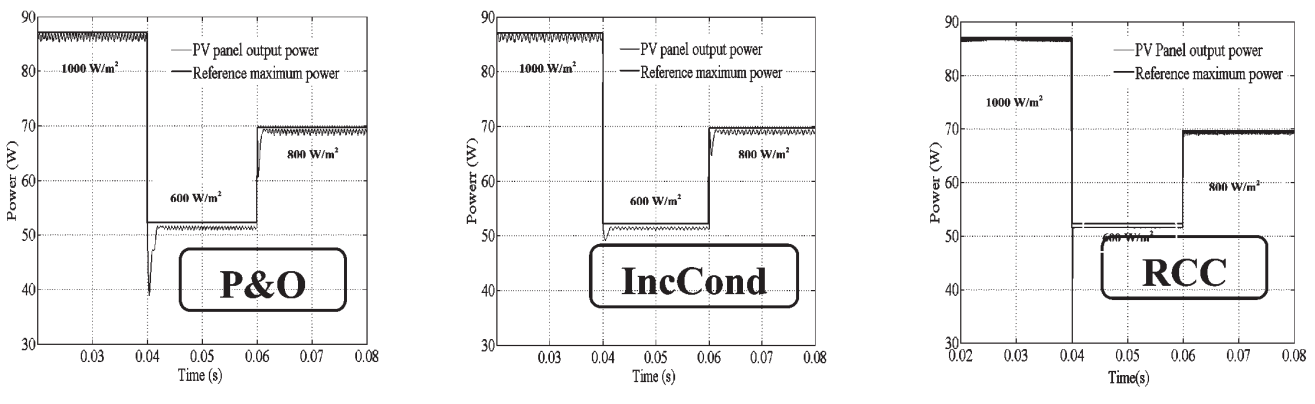

FIG. 10 POWER EXTRACTED FROM PV PANEL WITH SELECTED MPPT TECHNIQUES

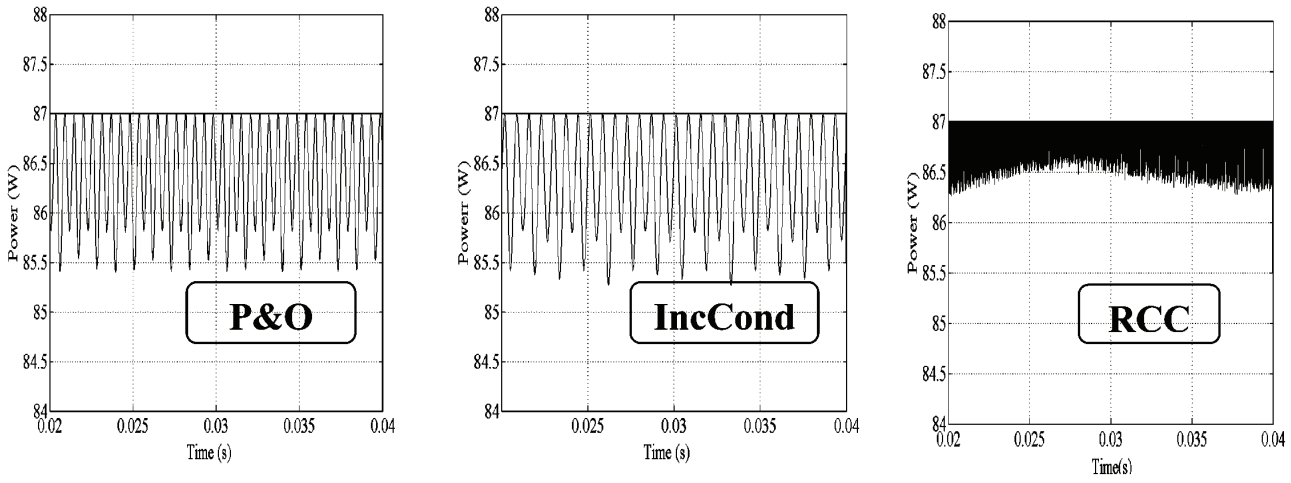

FIG. 11 POWER RIPPLE IN STEADY STATE

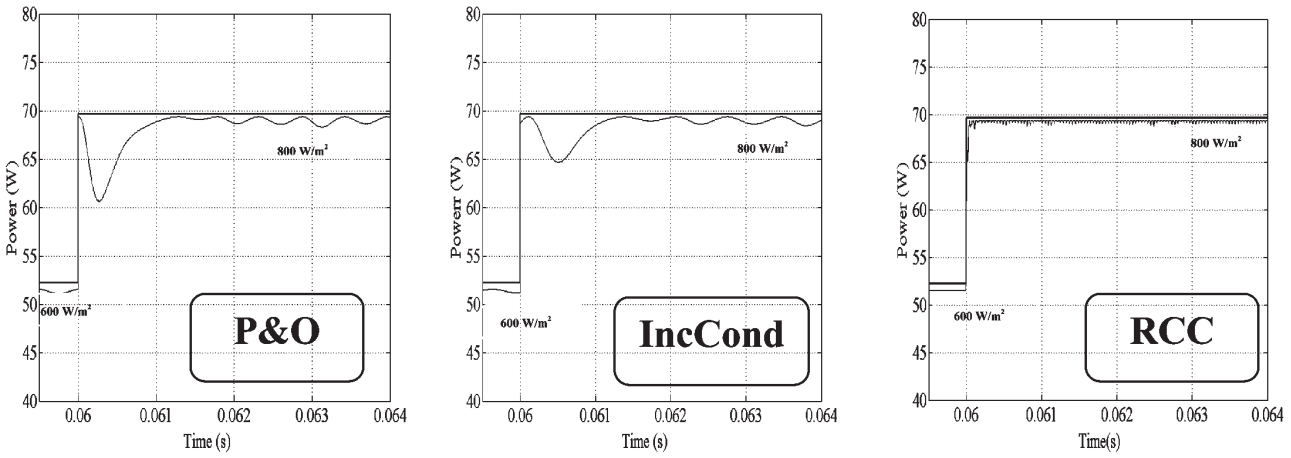

FIG. 12 MPPT DYNAMIC BEHAVIOR WITH STEP CHANGE IN INSOLATION

The power extracted from PV panel with the selected MPPT techniques with step change in insolation level at constant temperature is shown in Figure 10. From the simulated performance it is seen that the power extracted from the PV panel with ZVS-PWM Cuk converter corresponds to the desired maximum power for a given insolation level. Ripple comparisons in steady state of the power extracted are shown in Figure 11, where P&O and IncCond methods standout for having the largest ripple in steady state as compared with the ripple exhibited by the RCC MPPT.

MPPT methods are also compared with respect to their dynamic response, i.e. how they behave when the PV panel is subjected to sudden variation in the insolation level. According to these results RCC stands out, which presents less time to reach steady state maximum operating power point.

The waveforms showing the performance of dc-dc Cuk converter with ZVS active clamping are presented. Figure 13 shows the simulated resonant inductor current and voltage across the resonant capacitor. The current through the main switch S_1 and the voltage across it are shown in Figure 14, and it is evident that the switch operates with ZVS and the voltage across it is clamped actively by clamping capacitor to $V_{ca} + V_c$. Figure 15 shows the simulated voltage across and current through the free-wheeling diode D_{fw} and it is evident that the switching transitions occur at zero voltage across it. The simulated waveforms of auxilary switch current and voltage across it are shown in Figure 16. From all the switching waveforms it is seen that the switch undergoes the switching transitions at zero voltage resulting in reduced switching loss.

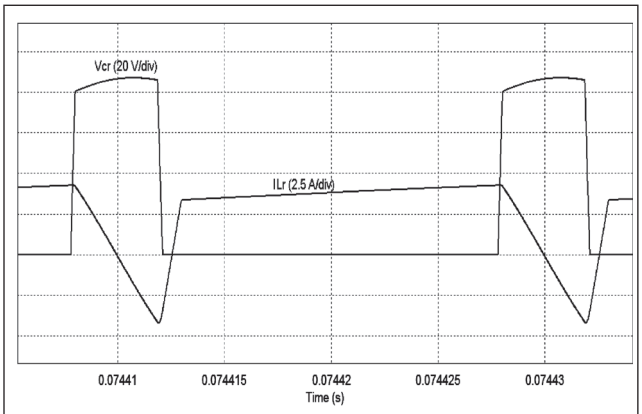

FIG. 13 VOLTAGE ACROSS C_R AND CURRENT THROUGH L_R

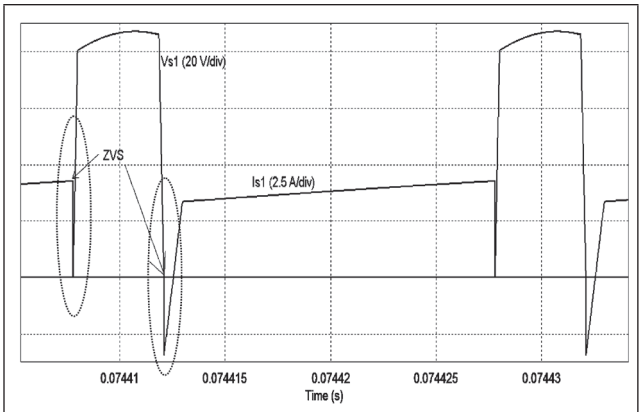

FIG. 14 VOLTAGE ACROSS AND CURRENT THROUGH MAIN SWITCH S_1.

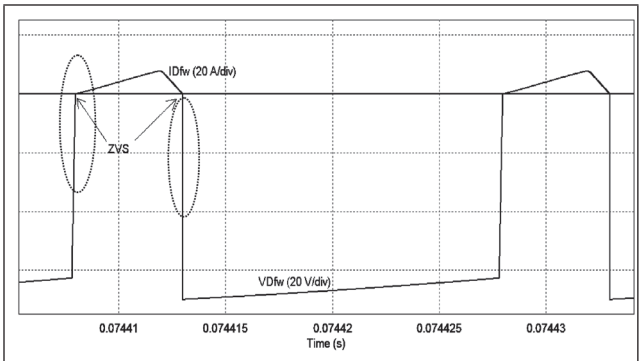

FIG. 15 VOLTAGE ACROSS AND CURRENT THROUGH D_{FW}

From the above waveforms, it is clear that the semiconductor devices of the PCS operate at ZVS with reduced switching losses results in high efficiency of power conversion, which confirms the efficient operation of converter at high frequencies with reduced size of reactive components and cost.

The converter presents high efficiency of 98% at full load.

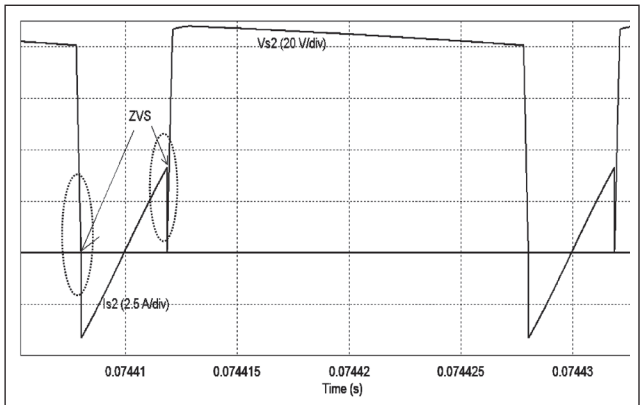

FIG. 16 VOLTAGE ACROSS AND CURRENT THROUGH SWITCH S_2.

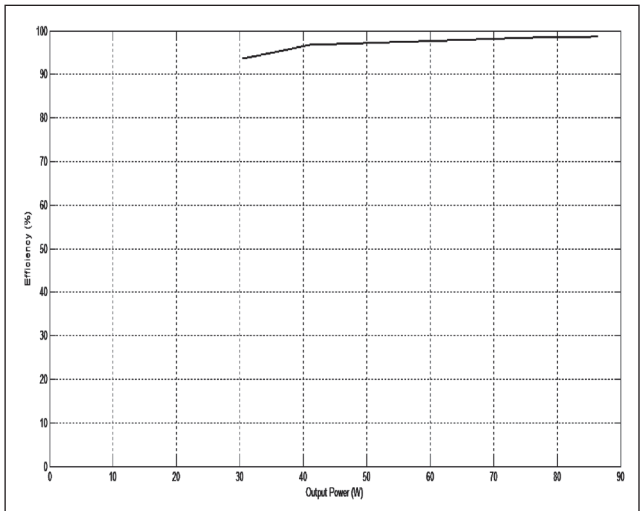

FIG. 17 EFFICIENCY CURVE WITH FIXED INSOLATION LEVEL FOR VARYING LOAD

TABLE 3

MAIN CHARACTERISTICS OF MPPT TECHNIQUES

MPPT method	Analog or Digital	Implementation Complexity	Tracking Time (ms)	Ripple at MPP (W)
P&O	Both	Low	1.8	2.5
IncCond	Digital	Medium	2.1	2.5
RCC	Analog	Low	0.4	1.5

5.0 CONCLUSION

High efficient dc-dc converters are being widely used in stand-alone PV lighting, solar cars and water pumping systems. In this paper the

operating principle, circuit design consideration of Cuk converter with active clamping and soft commutation (ZVS) have been presented. The MPPT techniques P&O, IncCond and RCC are applied to ZVS-PWM Cuk converter and the performance of operation is demonstrated. The dynamic performance of these MPPT techniques with step change in insolation levels is presented. The choice of MPPT scheme is application specific. Overall, the RCC method is the fastest and will particularly be suitable for fast changing environmental conditions further it is parameter insensitive and its application is independent of panel configuration. However it suffers from the lower tracking capability, particularly at low insolation levels, as it uses large step size near MPP. It is noted that the P&O and IncCond also deserve to be mentioned as alternatives for outstanding performance. It is seen that the difference in performances among the selected MPPT are very slight and a different PCS may render different values of the performance parameters, however it is expected that the variation remains less intact.

From the analytical and simulation studies the following conclusions are drawn

a) Soft commutation (ZVS) operation of the main and auxiliary switches is achieved.

b) The converter is controlled by conventional PWM technique operating at fixed switching frequency.

c) The converter is suitable for MPPT of PV system operating at high-frequency with high efficiency.

Simulation results confirm the viability and feasibility of the ZVS-PWM active clamped Cuk converter with high rate of convergence RCC MPPT for solar PV generation system.

Future work is aimed at designing experimental prototype for the proposed system.

REFERENCES

[1] F. Blaabjerg, R. Teodorescu, M. Liserre, and A. V. Timbus, “Overview of Control and Grid Synchronization for Distributed Power Generation Systems,” IEEE Trans. Ind. Electron., vol. 53, no. 5, pp. 1398-1409, Oct. 2006.

[2] T. Esram and P. L. Chapman, “Comparison of photovoltaic array maximum power point tracking techniques,” IEEE Trans. Energy Conv, vol. 22, no. 2, pp. 439-449, Jun. 2007.

[3] A. Safari and S.Mekhilef, “Simulation and hardware implementation of incremental conductance MPPT with direct control method using Cuk converter,” IEEE Trans. Ind. Appl., vol. 58, no. 4,pp. 1154-1161, Apr. 2011.

[4] H. Taghvaee, M.A.M.Radzi, S. M. Moosavain, Hashim Hizam, M.Hamiruce Marhaban, “A current and future study on non-isolated DC– DC converters for photovoltaic applications,” Renewable and Sustainable Energy Reviews, Elsevier vol. 17, pp. 216–227, Jan. 2013.

[5] M. G. Villava, J. R. Gazoli and E. R. Filho, “Comprehensive approach to modeling and simulation of photovoltaic modules,” IEEE Trans. Power. Electron., vol. 24, no. 5, pp. 1198-1208, May. 2009.

[6] D. B. Costa and C. M. C. Duarte, “The ZVS-PWM active clamping Cuk converter,”. IEEE Trans. Ind. Electron., vol. 51, no. 1, pp. 54-59, Feb. 2004.

[7] C. M. C. Duarte and I. Barbi, “A new family of ZVS –PWM active-clamping dc to dc boost converters: Analysis, design and experimentation ,” IEEE Trans. Power. Electron., vol. 12, no. 5, pp. 824-831, Sep. 1997.

[8] M.A.G. Brito, L.G. Junior, L.P. Sampaio, C.A.Canesin."Evaluation of MPPT Techniques for Photovoltaic Applications", IEEE Trans. Ind. Electron., vol. 60, no. 3, pp. 1156-1167, Mar. 2013.